Indonesian Physical Review

Volume 5 Issue 2, May 2022

P-ISSN: 2615-1278, E-ISSN: 2614-7904

Thickness Optimization of Organic Solar Cell by Optical and 1D Drift-Diffusion Electrical Modeling

Anjar Taufik Hidayat

Faculty of Telecommunication and Electronics Engineering, Institut Teknologi Telkom Purwokerto, Indonesia. E-mail: anjar@ittelkom-pwt.ac.id

ARTICLE INFO

Article info:

Received: 16-04-2022

Revised: 07-05-2022

Accepted: 12-05-2022

Keywords :

Drift-Diffusion Model; Film Thickness; GPDM; Hole Selective Layer; Organic Solar Cell; Power Conversion Efficiency; P3HT:PCBM

How To Cite :

Hidayat, A. T. (2022). Thickness Optimization of Organic Solar Cell by Optical and 1D Drift-Diffusion Electrical Modeling. Indonesian Physical Review, 5(2), 116-129

DOI :

https://doi.org/10.29303/ipr.v5i2.149

ABSTRACT

Finding the best thickness combination of the active layer and the interlayer of organic solar cells is essential to optimizing and producing an efficient device. In this research, the thickness combination was graphed by two scan steps, i.e., the major scan (50 nm - interval) followed by the minor scan (10 nm - interval). The solar cell device was modeled by optical and 1D drift-diffusion modeling in the gvdm simulation software with P3HT:PCBM as the active layer and three different materials for the hole-selective layer (interlayer). The best power conversion efficiencies were 5.21, 4.14, and 5.22% when PEDOT:PSS, V_2O_5, and Spiro-OMeTAD were interlayer materials. The effective thickness for every interlayer material is 10 nm, while the effective thickness of the active layer is 220 nm (for PEDOT:PSS and Spiro-OMeTAD devices) and 230 nm (for V_2O_5 device). As a result, each device gives higher power conversion efficiency than that from the original setting of the software. Furthermore, this study's highest power conversion efficiency was higher than previously reported. These results suggest that scanning a more extensive range of layer thickness combinations is necessary to find the highest power conversion efficiency possible for every organic solar cell device.

Introduction

Organic Solar Cells (OSCs) have enormous potential as an alternative to their inorganic counterparts owing to the low-cost, lightweight, easy-processed, and less environmental impact [1]–[4]. However, one primary challenge to being commercially available is their relatively low power conversion efficiencies (PCEs) compared to other types of solar cells, perovskite solar cells, for example [5]–[7]. For this challenge, tremendous advances have been made toward high PCE in the past few years. One result is the reported 18.2% PCE of single-

junction OSC [8]. The high value of PCE comes from the optimization of photocurrent generation steps, i.e., light absorption, exciton splitting, charge transport, and charge collection [9]. Light absorption, exciton splitting, and charge transport occur in the active layer, while interlayers transport charges collected by electrodes.

The active layer exposes a blend of p- and n-type organic materials by transmitted photons and generates excitons (electron-hole pairs). Interlayers are layers that lie between the active layer and electrodes. These layers provide ohmic contact to the electrodes and act as charge carrier selective layer (hole-selective layer (HSL) to block electrons and electron selective layer to block holes). Those processes are highly correlated with the film thickness.

The thicker active layer enables more excitons to be generated. On the contrary, a thicker layer improves charge carrier recombinations (electrons and holes relaxed to the neutral state) [10]. On the other hand, thicker HSL/ESL enables better electron/hole blocking but decreases photon transmittance in ordinary/inverted OSCs. The combination of active and interlayers are also an essential factor because each gives a different value of PCE. Therefore, the thickness of each layer and the thickness combination should be appropriately adjusted to produce high PCE.

A common strategy to optimize layer thickness is by setting a value to one layer and varying the thickness of another layer, and vice versa. This strategy could produce a high PCE value. However, the highest PCE value would only be found if all thickness combinations were tried. 2 or more steps can simplify this vast task. The first is by the rough scan with large intervals followed by another step with smaller intervals to the specific thicknesses range, giving a high PCE value. Even though the task could be simplified, making many samples according to the thickness combination is exhausting.

Those exhausting laboratory works can be replaced by using simulation software. The general-purpose photovoltaic device model (gpvdm) is a modeling software to build and analyze solar cells and other optoelectronic devices (OLEDs and OFETs). The electrical modeling in GPVDM is 1D/2D drift-diffusion model [11]. The correctness of the software has been proven by reported research [12]–[19]. Some reports have used gpvdm software to simulate OSCs without trying a larger range of thickness combinations [20]–[27].

This research demonstrates film thickness optimization of the ordinary single-junction OSCs with P3HT:PCBM as an active material and three kinds of HSL (PEDOT:PSS, V_2O_5, and Spiro-OMeTAD) by gpvdm simulation software. To find the maximum PCE, we use two types of scanning thickness combination processes, i.e., a significant scan with a 50 nm – interval and a minor scan with a 10 nm – interval. This research proves that using a more extensive range of thickness combinations is necessary to find better PCEs. Furthermore, the values of PCEs were compared to the result from the original setting of the software and previously reported PCEs.

Theory and Calculation

The electrical stimulation in this research was conducted by gpvdm software. This software uses a finite-difference drift-diffusion model for free carrier transport. Carrier trapping/de-

trapping is also accounted for by discretizing each mesh point in the drift-diffusion model energy space between the HOMO and LUMO [11].

The single-junction device consists of layers, i.e., contact, inter-, active, and the contact layer. All layers will interact with light. However, the only active layer is electrically active, and the carrier transport is modeled in detail by the drift-diffusion model. In this model, the active layer was treated as one material with the HOMO level from the p-type material and LUMO level from the n-type material. The model is described in short below.
The J_{sc} of the device is obtained by the photocurrent densities [24]:

$$J_{sc}(V) = \int_0^{\infty} \{J_p(\lambda, V) + J_n(\lambda, V)\}\, d\lambda \quad (1)$$

Where $J_p(\lambda, V)$ and $J_n(\lambda, V)$ hole and electron current density:

$$J_p(\lambda, V) = \frac{e}{W}\left\{\mu_p F \int_0^W \delta_p\, dx - D_p \int_0^W \frac{\partial \delta_p}{\partial x} dx\right\} \quad (2)$$

$$J_n(\lambda, V) = \frac{e}{W}\left\{\mu_n F \int_0^W \delta_n\, dx - D_n \int_0^W \frac{\partial \delta_n}{\partial x} dx\right\} \quad (3)$$

While the continuity equation is:

$$\frac{\partial}{\partial t}(\delta_n) = \mu_n F \frac{\partial}{\partial x}(\delta_n) + D_n \frac{\partial^2 \delta_n}{\partial x} + G e^{-X\alpha(\lambda)} - \frac{\delta_n}{\tau_n} = 0 \quad (4)$$

Where δ_n is the concentration of generated electrons, μ_n is electron mobility, F is the equation that shows the electric field in the cell, D_n Is the electron diffusion, and G is the optical generation rate of the carrier. Equation resolving and device modeling was described in detail in [28]–[30].

The trapping/de-trapping process relates to the Density of the States (DoS) of the active layer and, therefore, to the gap energy between the blend materials (n-type and p-type) [24]. The DoS parameters in this research are presented in Table 1. Unfortunately, organic materials have no standard DoS parameters (depending on fabrication conditions). Therefore, the parameters in this research were obtained from the software default parameters.

Table 1. The density of states (DOS) parameters of the active layer in the simulation

Parameters	Values	SI units
Electron trap density	3.80×10^{26}	$m^{-3}eV^{-1}$
Hole trap density	1.45×10^{25}	$m^{-3}eV^{-1}$
Electron tail slope	0.04	eV
Hole tail slope	0.06	eV
Electron mobility	2.48×10^{7}	$m^2V^{-1}s^{-1}$
Hole mobility	2.48×10^{7}	$m^2V^{-1}s^{-1}$
Relative permittivity	3.8	au
Number of traps	20	Bands
Free electron to trapped electron	2.50×10^{20}	m^{-2}
Trapped electron to free hole	1.32×10^{22}	m^{-2}
Trapped hole to free electron	4.67×10^{26}	m^{-2}
Free hole to trapped hole	4.86×10^{22}	m^{-2}

Effective desity of free electron states (@300K)	1.28×10^{27}	m^{-3}
Effective desity of free hole states (@300K)	2.86×10^{25}	m^{-3}
Affinity	3.8	eV
Gap energy	1.1	eV
Recombination rate constant	0.0	$m^3 s^{-1}$

The solar cell device parameters are written as follows. The V_{oc} is:

$$V_{oc} = \frac{nkT}{q} \times \ln\left(\frac{J_{pki}}{J_0} + 1\right) \quad (5)$$

With n is the ideality factor, k is the Boltzmann constant, T is temperature, q is the electron charge density, and J_0 saturation current density.

The fill factor of the cell is calculated by:

$$FF = \frac{J_{mp}V_{mp}}{J_{sc}V_{oc}} \quad (6)$$

The following equation calculates the Power Conversion Efficiency:

$$PCE = \frac{J_{sc}V_{oc}FF}{P_{in}} \quad (7)$$

where P_{in} Power input.

The device area in this study is 6 mm^2. The device was tested under 1.5 AM with 1 sun (W/m^2).

Experimental Method

Materials

The p-type: n-type material blend for the active layer in this experiment is P3HT:PCBM (Fig. 1(a) and (b)). This type of blend is widely studied and has become a standard model in the research field of organic solar cells [9]. On the other hand, three kinds of HSL (Fig. 1(c), (d), and (e)), namely PEDOT:PSS (polymer), V_2O_5 (Oxides), and Spiro-OMeTAD (small molecules), were incorporated separately in each device to form ohmic contact as well as blocking layer for the generated electrons from the active layer.

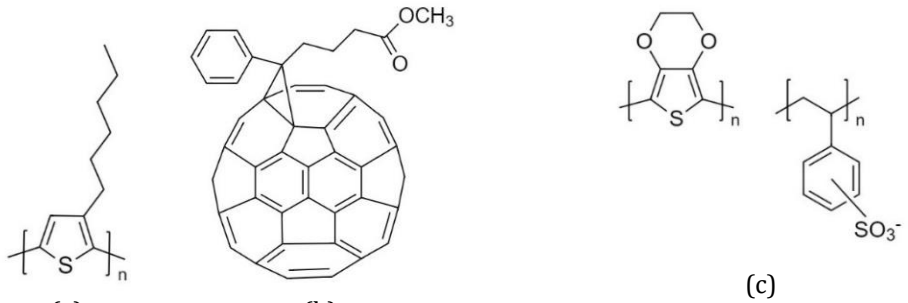

(a) (b) (c)

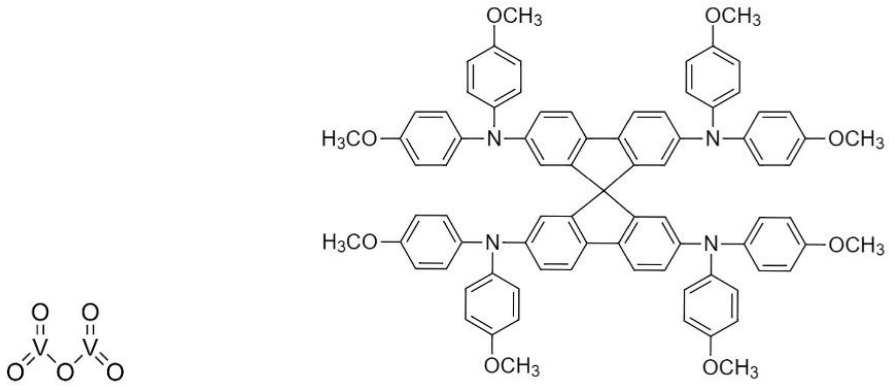

(d) (e)

Figure 1. Chemical structure of: (a) P3HT, (b) PCBM, (c) PEDOT:PSS, (d) V_2O_5, and (e) Spiro-OMeTAD. The chemical structures in the figure are generated by ChemDraw Website [31].

Device structure

The HSL and the active layer were sandwiched between Al and ITO. The transparent ITO becomes the top electrode and faces the light source. Photons (green wavy arrow in Figure 2) transmitted to and generated electrons and holes in the active layer from the top. The electrons and holes were collected in the ITO and Al electrodes. The thickness of HSL and the active layer will be studied. The Thickness of both ITO and Al electrodes was set to 100 nm. ITO electrodes were chosen due to the transparency, while Al electrodes were chosen due to the shallow energy level and the ability to form ohmic contact without interlayer.

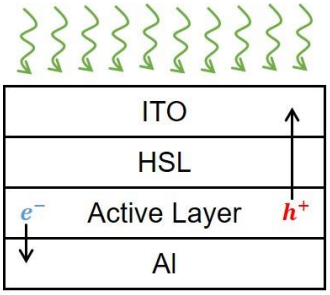

Figure 2. The device structure of the single-junction OSC device in this research.

Strategy to find efficient layer thickness

An efficient layer thickness combination is a combination of active layer and HSL, which gives the highest PCE. The combination was scanned by the major and followed by the minor scan. At first, PEDOT:PSS was set as HSL. The major scan was (1) the thickness of the HSL was kept at 50 nm, and the thickness of the active layer was varied by: 50, 100, 150, 200, 250, 300, 350, 400, 450, 500, 550, and 600 nm. All results were saved in the spreadsheet. (2) the same steps were applied for the following HSL thickness: 50, 100, 150, 200, 250, and 300 nm. (3) the PCE data was then graphed to see the trend. The values of the effective thickness range will appear at around the highest PCE. The thickness range was marked by gray color.

The minor scan was the next step to find the more effective thickness combination by scanning the previous effective range (gray color) at 10 nm. The same procedure was applied to V_2O_5 and Spiro-OMeOTAD for HSL.

Result and Discussion

The results are presented separately depending on the type of HSL used. Therefore, "PEDOT:PSS device" is a term to refer to the device in which PEDOT:PSS was used as HSL material. Other terms are V_2O_5 and Spiro-OMeTAD devices.

PEDOT:PSS Device

Figure 3 was generated from the simulation data with PEDOT:PSS as an HSL and P3HT:PCBM as an active layer. The active layer thickness and PCE are presented on the x and y-axis, while the colored graphs are related to HSL film thickness. A higher PCE value represents a more efficient film thickness combination. The figure has major and minor scan clusters, represented by square plot – dashed line and circle plot – solid line, respectively. The major scan is scanning maximum PCE with a 50 nm – interval for HSL and active layer thickness, and the thickness range is 50-600 nm for the active layer and 50-300 nm for the HSL. The minor scan is scanning maximum PCE with a 10 nm – interval for both HSL and active layer. The thickness range for the minor scan depends on the HSL materials.

In the major scan, all graphs have fairly the same trend. The value of PCE goes up and down before and after 200 nm. Therefore, the maximum PCE for each HSL thickness lies between 150-250 nm (a gray area in Fig. 3). On the other hand, a thinner layer of HSL seems to produce a more efficient device. Therefore, maximum PCE appears to come from the thickness of the active layer, less than 50 nm.

Based on the previous explanation, the range for the minor scan is 150-250 nm for the active layer and 10-50 nm for the HSL. In the minor scan, all graphs seem to follow the same trend. The PCE goes up and down before and after 230 nm except for 10 nm – thick HSL (red-colored). The red-colored graph has the maximum PCE when the thickness of the active layer is 220 nm. Therefore, a 10 nm HSL and 220 nm active layer is the most efficient combination based on Fig. 3 with the PCE value of 5.21%. This value is higher than the 4.63% PCE from the default setting of the software with 220 nm – active layer and 10 nm - HSL.

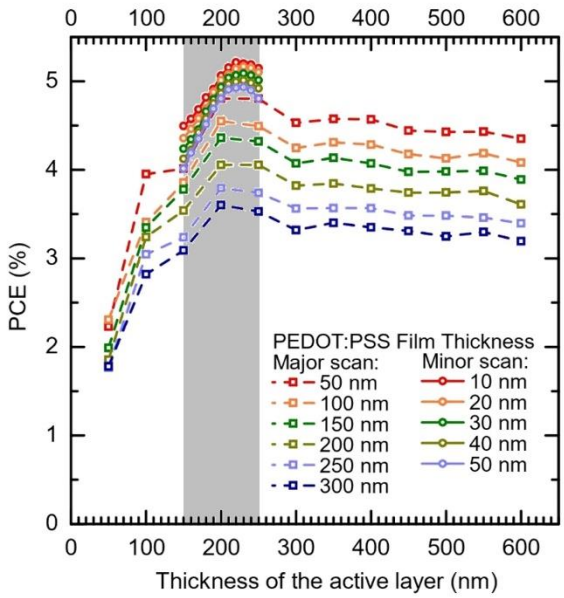

Figure 3: Efficient PEDOT:PSS and the active layer thickness.

V_2O_5 Device

The graphing figure to scan the efficient thickness combination of V_2O_5 as HSL material and P3HT:PCBM as the active layer is presented in Figure 4. The x and y-axis are the Thickness of the active layer and PCE, respectively, while the colored graphs are the thickness of HSL. The major and minor scans were presented as the square plot – dashed line and circle plot – solid line, respectively.

It is difficult to say that there is a trend between the major scan graphs since the distances are significant. However, it is safe to say that the efficient thickness would be at a 200 – 300 nm thick active layer (a gray area in Fig. 6). On the other hand, efficient thickness for the HSL would be at a range lower than 50 nm. Therefore, the minor scan was applied at 200-300 nm for the active layer and 10-50 nm for the HSL.

In the minor scan, there is no similar shape between the graphs. However, the thinner HSL is better for getting higher PCE. For example, in the thinnest HSL (red-colored), the maximum PCE is yielded from 230 nm – active layer thickness. Therefore, the efficient thickness combination is 10 nm HSL and 230 nm active layer with the PCE value of 4.14%. This value is higher than 0.67%-PCE from the original setting of the software with 220 nm – active layer and 100 nm - HSL.

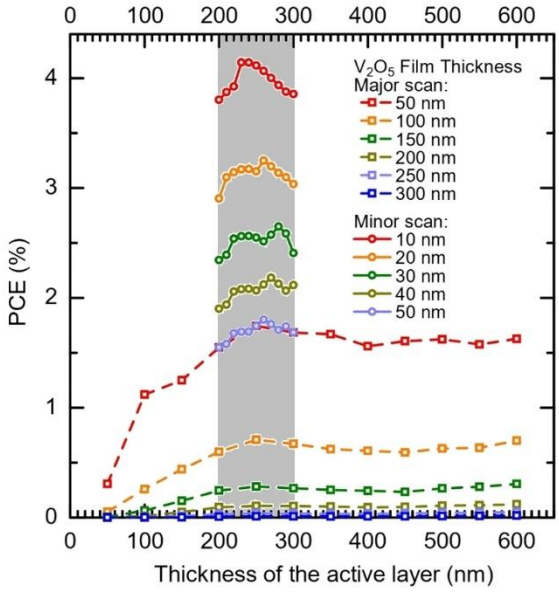

Figure 4: Efficient V_2O_5 and the active layer thickness.

Spiro-OMeTAD Device

Figure 5 shows the graphs to find an efficient thickness combination of Spiro-OMeTAD as HSL and P3HT:PCBM as an active layer to produce a maximum value of PCE. The x and y-axis are the Thickness of the active layer and PCE, respectively, while the colored graphs are the Thickness of HSL. The major and minor scans were presented as the square plot – dashed line and circle plot – solid line, respectively.

In the major scan, every graph reasonably follows the same trend where the value of PVE goes up and down with a 250 nm – thick active layer as a peak. Therefore the maximum PCE is 200-300 nm active layer. On the other hand, thinner HSL seems favorable to producing higher PCE. Therefore, the efficient HSL thickness should be around 10-50 nm.

The range for the minor scan is 200-300 nm for the active layer and 10-50 nm for the HSL. In the minor scan, all graphs follow the same trend where 230 nm – active layer thickness is a peak except for the 10 nm – HSL thickness graph (red-colored). In the red graph, the maximum value of PCE is formed by 220 nm – active layer thickness. Therefore, the efficient thickness combination is 10 nm HSL and 220 nm active layer with a PCE value of 5.22%. This value is higher than 4.92% PCE from the original setting of the software with 220 nm – active layer and 100 nm – HSL.

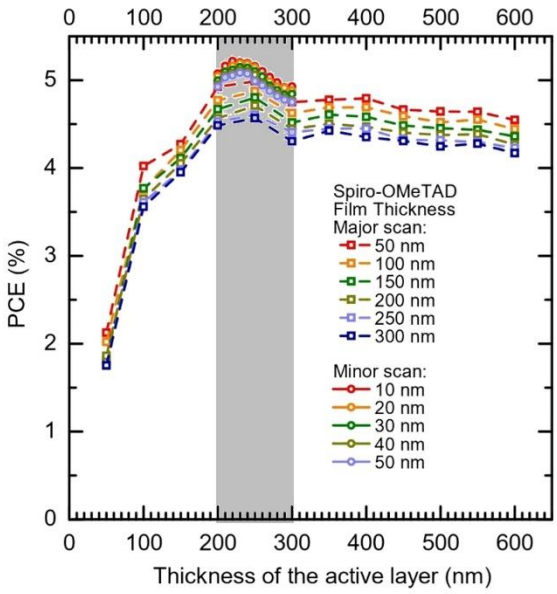

Figure 5: Efficient Spiro-OMeTAD and the active layer thickness.

Comparison Between Devices

Table 2 shows a scanning comparison between devices. The major scan for all combinations is the same but not for the minor scan. This minor scan result is a peak that corresponds to the effective layer thickness and maximum PCE. The effective HSL thickness for all devices is the same. However, the effective active layer thicknesses are the same for PEDOT:PSS and Spiro-OMeTAD devices and slightly less effective for V_2O_5 devices.

The effective Thickness of all HSL is 10 nm of all HSL. This value is considerably thin in the research field and the lowest range. This phenomenon might have come from the transparency of the HSL layer since this layer is on the active layer (see Fig. 2). The light from the source passed the ITO and HSL before it reached the active layer. Therefore, thin HSL is favorable for producing better PCE.

The software's default layer thickness for P3HT:PCBM active material is 220 nm. This value is valid for PEDOT:PSS and Spiro-OMeTAD devices but not V_2O_5 devices. The best PCE value for the V_2O_5 device comes from 230 nm-thick active material. From this difference, it can be concluded that the default thickness setting from the software is not always the best. It is due to the device's performance related to the active and interlayer layers. Therefore, different materials combinations might have different outcomes, and the scanning thickness combination process is necessary to find maximum PCE.

The best PCE in Table 2 are from PEDOT:PSS and Spiro-OMeTAD devices. Both have 220 nm – active layer thickness and yield the exact value of 5.2% PCE. The same value of PCE some from the value of photogenerated current (Figure 6 and Table 3). However, the scanning figure between the two have different characteristics (see Figures 3 and 5). These differences might

come from the optical characteristics between the two. For example, figure 7 shows the largest bandgap of Spiro-OMeTAD among three HSL materials, which correspond to the better light transmission [23]. However, there is a slight difference in the HOMO level of Spiro-OMeTAD and the active layer. This small energy barrier might hinder the Spiro-OMeTAD device from having the best PCE.

As expected, the highest 5.22% PCE in this experiment is higher than the previously reported value with the P3HT:PCBM active layer by using the same device structure (4.5% [20], 4.59% [21], 4.35% [22]). Even though some references also use electron selective layer (ESL), the values are still lower than PCE in this experiment (5.02% [23], 5.14% [24], 5% [25], 5.03% [26], 3.9% [27]). From these comparisons, it can be concluded that the scanning process is needed to attain maximum PCE and get the best thickness combination of active layer and HSL.

Table 2: Scanning comparisons

Materials for HSL	Minor scan (nm)		Effective Thickness (nm)		Maximum PCE (%)
	HSL	Active Layer	HSL	Active Layer	
PEDOT:PSS	10 – 50	150 – 250	10	220	5.21
V_2O_5	10 – 50	200 – 300	10	230	4.14
Spiro-OMeTAD	10 – 50	200 – 300	10	220	5.22

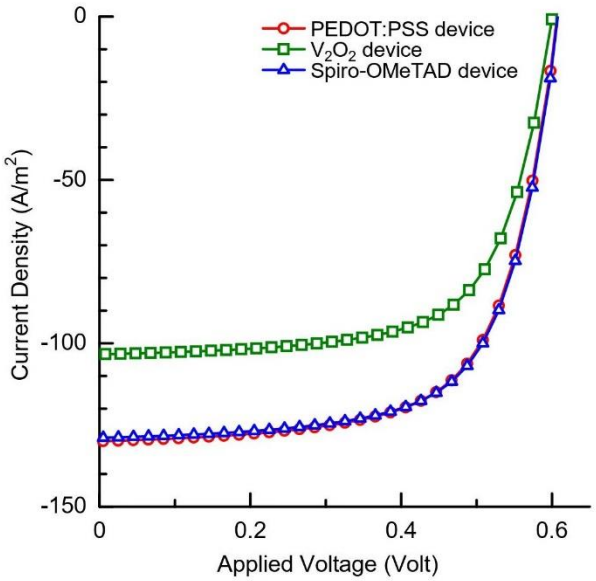

Figure 6: J-V characteristics from the simulation by using adequate film thickness for each device

Table 3: Solar cell parameter comparisons

Materials for HSL	J_{SC}	V_{OC}	FF	PCE (%)
PEDOT:PSS	-128.756	0.607592	0.6663	5.21
V_2O_5	-103.3256	0.600358	0.667763	4.14
Spiro-OMeTAD	-128.8917	0.607615	0.666138	5.22

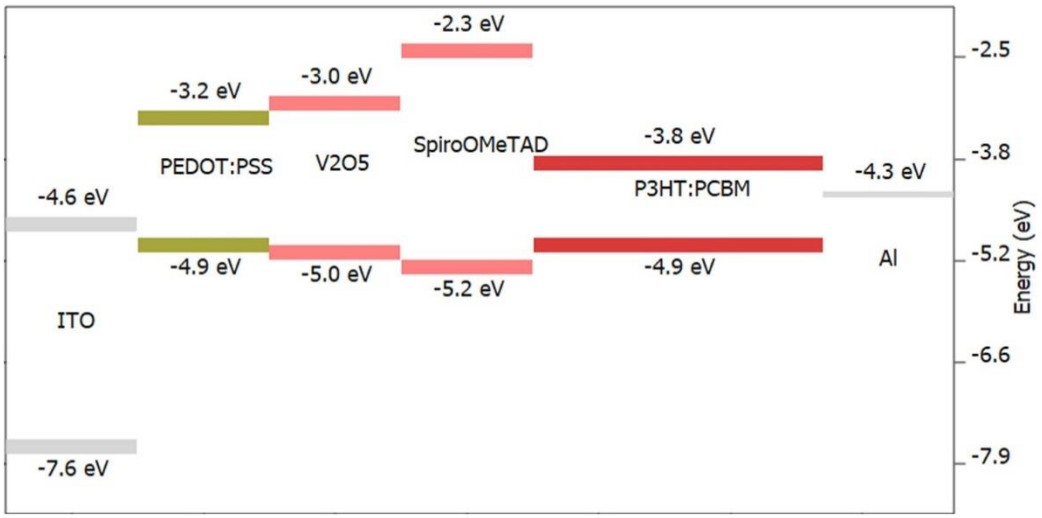

Figure 7: Energy level comparison between materials. Gpvdm generated this image with energy level values from previous experiments [32]–[35] except for the software's active layer.

Conclusion

This research proves that using a larger range of thickness combinations is necessary to find better PCEs. The thickness combination of the active layer and HSL was scanned with a major scan followed by a minor scan. From these scans, the best thickness combination of the active layer and HSL was marked by the highest value of PCE. The best PCEs are 5.21, 4.14, and 5.22% for PEDOT:PSS, V_2O_5, and Spiro-OMeTAD devices, respectively. Those PCEs were generated from 10 nm as the effective Thickness of HSL, while the effective thickness of the active layer is 220 nm (for PEDOT:PSS and Spiro-OMeTAD devices) and 230 nm (for V_2O_5 device). Each device gives a higher PCE than that from the original setting of the software. The PCE in this study was also higher than that previously reported. These results prove that scanning a larger range of layer thickness combinations is necessary to find the highest PCE for every OSC device.

This study is limited to single junction OSC by using only HSL as an interlayer (without ESL). However, this study shows the importance of scanning thickness combinations in a larger range to produce the highest possible PCE. The scan was represented in a 2D graph using PCE, HSL thickness, and active layer thickness. Further study is necessary for scanning the best combination of the active layer, HSL, and ESL (four parameters) by using better data visualization.

References

[1] L. X. Chen, "Organic Solar Cells: Recent Progress and Challenges," *ACS Energy Lett.*, vol. 4, no. 10, pp. 2537–2539, 2019.

[2] Y. Tamai, H. Ohkita, H. Benten, and S. Ito, "Exciton Diffusion in Conjugated Polymers: From Fundamental Understanding to Improvement in Photovoltaic Conversion

Efficiency," *J. Phys. Chem. Lett.*, vol. 6, no. 17, pp. 3417–3428, Sep. 2015.

[3] H. Benten, D. Mori, H. Ohkita, and S. Ito, "Recent research progress of polymer donor/polymer acceptor blend solar cells," *J. Mater. Chem. A*, vol. 4, no. 15, pp. 5340–5365, 2016.

[4] H. Benten, T. Nishida, D. Mori, H. Xu, H. Ohkita, and S. Ito, "High-performance ternary blend all-polymer solar cells with complementary absorption bands from visible to near-infrared wavelengths," *Energy Environ. Sci.*, vol. 9, no. 1, pp. 135–140, 2016.

[5] N. Pandey, A. Kumar, and S. Chakrabarti, "Investigation of the structural, electronic, and optical properties of Mn-doped CsPbCl3: theory and experiment," pp. 29556–29565, 2019.

[6] A. Kumar, N. Pandey, S. Dongre, and S. Chakrabarti, "Green light emission in CsPbBr3 quantum dots: theoretical and experimental insight," in *Light-Emitting Devices, Materials, and Applications XXIV*, 2020, p. 66.

[7] N. Marinova, S. Valero, and J. Luis, "Organic and perovskite solar cells: Working principles, materials and interfaces," *J. Colloid Interface Sci.*, vol. 488, pp. 373–389, 2017.

[8] Best-Research-Cell-Efficiencies-Rev210726.Pdf. [Online]. Available: https://www.nrel.gov/pv/assets/pdfs/best-research-cell-efficiencies-rev220126.pdf.

[9] C. Brabec, U. Scherf, and V. Dyakonov, *Organic Photovoltaics: Materials, Device Physics, and Manufacturing Technologies, 2nd Edition*. Wiley-VCH, 2014.

[10] D. Zhang *et al.*, "Recent progress in thick-film organic photovoltaic devices: Materials, devices, and processing," *SusMat*, vol. 1, no. 1, pp. 4–23, 2021.

[11] R. C. I. MacKenzie, "Understanding gpvdm v7.88," 2022. [Online]. Available: http://gpvdm.com.

[12] A. bdelkade. Hima, "GPVDM simulation of layer thickness effect on power conversion efficiency of CH3NH3PbI3 based planar heterojunction solar cell," *Int. J. Energ.*, vol. 3, no. 1, p. 37, 2018.

[13] N. Singh, A. Chaudhary, S. Saxena, M. Saxena, and N. Rastogi, "Electrical Simulation of Organic Solar Cell at Different Charge Carrier Mobility," *IOSR J. Appl. Phys.*, vol. 09, no. 02, pp. 01–04, 2017.

[14] H. Abdulsalam, G. Babaji, and H. T. Abba, "The Effect of Temperature and Active layer thickness on the Performance of CH 3 NH 3 PbI 3 Perovskite Solar Cell: A Numerical Simulation approach," *Sci. Front Publ. J. Found. Appl. Phys.*, vol. 5, no. 2, pp. 141–151, 2018.

[15] R. C. I. Mackenzie *et al.*, "Loss Mechanisms in High Efficiency Polymer Solar Cells," *Adv. Energy Mater.*, vol. 6, no. 4, pp. 2–8, 2016.

[16] Y. Gao, R. C. I. MacKenzie, Y. Liu, B. Xu, P. H. M. Van Loosdrecht, and W. Tian, "Engineering Ultra Long Charge Carrier Lifetimes in Organic Electronic Devices at Room Temperature," *Adv. Mater. Interfaces*, vol. 2, no. 4, pp. 1–7, 2015.

[17] Y. Liu *et al.*, "Organic semiconductors with a charge carrier life time of over 2 hours at room temperature," *J. Mater. Chem. C*, vol. 3, no. 47, pp. 12260–12266, 2015.

[18] L. Sims *et al.*, "Investigation of the s-shape caused by the hole selective layer in bulk heterojunction solar cells," *Org. Electron.*, vol. 15, no. 11, pp. 2862–2867, 2014.

[19] R. Hanfland, M. A. Fischer, W. Brütting, U. Würfel, and R. C. I. Mackenzie, "The physical meaning of charge extraction by linearly increasing voltage transients from organic solar cells," *Appl. Phys. Lett.*, vol. 103, no. 6, 2013.

[20] R. Islam, M. M. Abrar, F. Hassan, and S. Adnan, "Layer thickness effect on power conversion efficiency of a P3HT:PCBM based organicsolar cell," *1st Int. Conf. Adv. Sci. Eng. Robot. Technol. 2019, ICASERT 2019*, vol. 2019, no. Icasert, pp. 1–3, 2019.

[21] K. Chakraborty, S. Malakar, D. K. Mandal, R. Mondal, and A. K. Maiti, "Experimental Prediction of Effect of Thickness of Active Layer of Photovoltaic Device on a series of Electrical Parameters using GPVDM Software," *Int. J. Adv. Sci. Eng.*, vol. 6, no. S1, pp. 42–46, 2019.

[22] K. L. Damena, "Investigation of Organic Solar Cell at Different Active Layer Thickness and Suns Using Electrical Simulation," vol. 6, no. 12, p. 1615, 2019.

[23] M. Abdallaoui, N. Sengouga, A. Chala, A. F. Meftah, and A. M. Meftah, "Comparative study of conventional and inverted P3HT:PCBM organic solar cell," *Opt. Mater. (Amst).*, vol. 105, p. 109916, Jul. 2020.

[24] S. Sen and R. Islam, "Effect of Different Layers on the Performance of P3HT:PCBM-Based Organic Solar Cell," *Brazilian J. Phys.*, vol. 51, no. 6, pp. 1661–1669, 2021.

[25] O. Ourahmoun, "Simulation of the Electrical Parameters of Organic Photovoltaic Cells under QUCS and GPVDM Software," *Wseas Trans. Circuits Syst.*, vol. 19, pp. 196–205, 2020.

[26] W. Farooq, A. D. Khan, A. D. Khan, and M. Noman, "Enhancing the power conversion efficiency of organic solar cells," *Optik (Stuttg).*, vol. 208, p. 164093, Apr. 2020.

[27] M. Erray, M. Hanine, E.-M. Boufounas, and A. El Amrani, "Effects of carriers charge mobility and work function on the performances of P3HT:PCBM based organic photovoltaic solar cell," in *2018 4th International Conference on Optimization and Applications (ICOA)*, 2018, pp. 1–6.

[28] R. C. I. MacKenzie, C. G. Shuttle, M. L. Chabinyc, and J. Nelson, "Extracting microscopic device parameters from transient photocurrent measurements of P3HT:PCBM solar cells," *Adv. Energy Mater.*, vol. 2, no. 6, pp. 662–669, 2012.

[29] R. C. I. MacKenzie, T. Kirchartz, G. F. A. Dibb, and J. Nelson, "Modeling nongeminate recombination in P3HT:PCBM solar cells," *J. Phys. Chem. C*, vol. 115, no. 19, pp. 9806–9813, 2011.

[30] F. Deschler, D. Riedel, B. Ecker, E. Von Hauff, E. Da Como, and R. C. I. MacKenzie, "Increasing organic solar cell efficiency with polymer interlayers," *Phys. Chem. Chem. Phys.*, vol. 15, no. 3, pp. 764–769, 2013.

[31] ChemDraw. [Online]. Available: https://chemdrawdirect.perkinelmer.cloud/js/sample/index.html#. [Accessed: 27-Mar-2022].

[32] B. Ofuonye, J. Lee, M. Yan, C. Sun, J. M. Zuo, and I. Adesida, "Electrical and microstructural properties of thermally annealed Ni/Au and Ni/Pt/Au Schottky contacts on AlGaN/GaN heterostructures," *Semicond. Sci. Technol.*, vol. 29, no. 9, 2014.

[33] P. Wangyang *et al.*, "Recent Advances in Halide Perovskite Photodetectors Based on

Different Dimensional Materials," *Adv. Opt. Mater.*, vol. 6, no. 11, pp. 1–30, 2018.

[34] G. Terán-Escobar, J. Pampel, J. M. Caicedo, and M. Lira-Cantú, "Low-temperature, solution-processed, layered V_2O_5 hydrate as the hole-transport layer for stable organic solar cells," *Energy Environ. Sci.*, vol. 6, no. 10, pp. 3088–3098, 2013.

[35] Y. Zhou *et al.*, "A Universal Method to Produce Low-Work Function Electrodes for Organic Electronics," vol. 873, no. April, pp. 327–332, 2012.